Available online at www.sciencedirect.com

ScienceDirect

Procedia Engineering 00 (2017) 000–000

SAND2017-3950C

Procedia Engineering

www.elsevier.com/locate/procedia

DYMAT 23rd Technical Meeting

Dynamic Fracture of Ductile Materials

Dynamic Characterization and Stress-Strain Symmetry of Vascomax® C250 Maraging Steel in Compression and Tension

Bo Song[a]*, Brett Sanborn[a], Peter E. Wakeland[a], Michael D. Furnish[a]

[a] *Sandia National Laboratories, 1515 Eubank SE, Albuquerque, NM 87122, USA*

Abstract

Low carbon, high strength steel alloys such as Vascomax steels are used in a wide variety of extreme environments due to their high strength, high fracture toughness, and stability over a wide range of temperatures. In this study, Vascomax® C250 steel was dynamically characterized in compression using Kolsky compression bar techniques at two strain rates of 1000 and 3000 s^{-1}. A pair of impedance-matched tungsten carbide platens were implemented to protect damage to the bar ends. The tungsten carbide platens were experimentally calibrated as system compliance which was then properly corrected for actual specimen strain measurements. In addition, elastic indentation of the high-strength compression sample into the platens was also evaluated and showed negligible effect on the specimen strain measurements. The Vascomax® C250 steel exhibited strain-rate effects on the compressive stress-strain curves. The dynamic yield strength was approximately 18% higher than quasi-static yield strength obtained from hardness tests. The dynamic true stress-strain curves of the Vascomax® C250 steel in compression were also computed and then compared with the previously obtained true tensile stress-strain curves at the same strain rates. The Vascomax® C250 steel exhibited a reasonable symmetry in dynamic compression and tensile stress-strain response. However, the fracture strains in dynamic compression were smaller than those in dynamic tension probably due to different fracture mechanisms in the different loading modes.

Peer-review under responsibility of [NAME OF THE ORGANIZATION].

Keywords: Vascomax® C250 steel, Kolsky bar, strain rate, stress-strain curve, dynamic compression, dynamic tension

* Corresponding author. Tel.: 1-505-844-4285
E-mail address: bsong@sandia.gov

Peer-review under responsibility of the scientific committee of the International Conference on Dynamic Fracture of Ductile Materials.

1. Introduction

Vascomax® maraging alloys are iron-based high strength steels but with low carbon content. Vascomax® C250 maraging alloy refers to the strengthened steel with ~7.8% cobalt. Such a maraging steel is usually relatively soft in annealed condition but can be hardened to very high strength through a precipitation hardening process at relatively low furnace temperatures [1]. Therefore, the Vascomax® C250 maraging alloy have been extensively utilized in a wide variety of extreme environments such as aerospace, manufacturing, tooling, transportation, and military applications, due to high strength, high fracture toughness, and stability over a wide range of temperatures. In these applications, the material may be subjected to high-speed impact or blast loading, which warrants investigation of mechanical properties including failure and fracture of the materials at elevated strain rates under various loading modes for mechanical design and modeling of impact events.

The Kolsky bar, also called a split Hopkinson bar, has been widely employed for dynamic material property characterization at high strain rates. The Kolsky bar was first developed in the compression mode by Kolsky in 1949 [2] and then in tension mode by Harding in 1960 [3]. Although the Kolsky compression and tension bars follow the same governing principles, unique challenges may exist between both configurations depending on the specimen material. Experimental challenges in dynamic tensile characterization of Vascomax® C250 alloy have been discussed and remedies were also presented in [4]. Major challenges in a Kolsky tensile bar experiment include 1) pseudo stress peak in the resultant stress-strain curve due to the threaded connection between the tensile specimen and the bar ends; and 2) accurate specimen strain measurement because the reflected pulse may be no longer reliable for specimen strain measurement due to multi-interfacial reflections between the specimen and the bar ends. Most recent study indicates that applying a lock nut to each threaded end of the tensile specimen removes the pseudo stress peak, which also reduces the effect of the interface on the reliability of the reflected pulse [4-7]. As such, the reflected pulse may still be valid for calculating specimen strain with the conventional method. Alternatively, laser extensometers for directly measuring specimen displacement have been developed for more precise small-strain measurement of the specimen [4, 7, 8]. Since dynamic tensile characterization of Vascomax® C250 alloy has been previously presented in Ref. [4], we will not focus on detail in the dynamic tensile technique in this paper.

Historically, the Kolsky compression bar technique has been utilized more extensively than the Kolsky tension bar technique [9]. For valid mechanical characterization, it is important to achieve stress equilibrium and constant strain rate in the specimen [9], which is commonly achieved via pulse shaping the incident pulse to a desired profile of so as to form a plateau in reflected pulse. The common pulse shaping technique is to apply a small piece of "tip" material, also called "pulse shaper", to the impact end of the incident bar [10, 11]. Upon impact of the striker, the pulse shaper is subjected to plastic deformation, thereby modifying the shape and amplitude of the incident pulse. Usually the rise time of the incident pulse determines the progress of stress equilibrium; whereas, the shape of the incident pulse determines if a constant strain rate is achieved. When the specimen stress is equilibrated, the plateau in the reflected pulse represents a constant strain rate. Stress equilibrium is usually assessed by comparing the stresses at both ends of the specimen. If the difference is within 5% of the mean value of the stresses at both ends of the specimen, the specimen stress is considered to be equilibrated [12]. Only after valid testing conditions are satisfied, can the resultant stress-strain curves be recognized as reliable, particularly the plastic flow region. It is more challenging to obtain a reliable elastic portion in Kolsky compression bar experiments on metallic materials. When testing a metallic specimen, the relatively high strength of the metallic specimen may generate elastic indentation into the bar ends, which results in inaccurate measurement of elastic response of the specimen material [13, 14]. Pulse shaping and numerical correction of elastic indentation have been found to be capable of obtaining more reliable elastic stress-strain response [14]. However, if the specimen material possesses a superior hardness, the specimen may generate plastic indentation into the bar ends. The plastic indentation not only damages the bar ends but also invalidates the Kolsky bar testing conditions. In order to prevent the bar ends from being indented or damaged, a pair of high-strength platens have been placed between the specimen and the bar ends when high-strength brittle materials, i.e., ceramics, are characterized with a Kolsky compression bar [15]. The platens are required to have similar mechanical impedance to the pressure bars to minimize the disturbance of stress wave propagation due to the introduction of the platens. However, it is difficult to make the mechanical impedance of the

platens perfectly match the pressure bars such that the stress wave may be disturbed to affect specimen strain measurement with the reflected pulse. Therefore, a more precise method of specimen strain/displacement measurement is desired.

In this study, we designed a pair of tungsten carbide platens confined with a stainless steel sleeve to protect the pressure bar ends from being damaged during dynamic testing. The resultant high-rate compressive stress-strain curves of the Vascomax® C250 alloy were compared with the dynamic tensile stress-strain curves to investigate the symmetry of dynamic material response in compression and tension.

Table 1. Chemical Compositions of Vascomax®C250 alloy

C	S	Mn	Si	Cr	Mo	Co	Ti	Al	B	Zr	Cu	P	W	Ni	Fe
0.005	0.0004	0.02	0.01	0.02	4.76	7.81	0.42	0.11	0.003	<0.01	<0.01	0.003	<0.01	18.55	BAL

2. Material and Compression Specimens

The chemical compositions for the Vascomax®C250 alloy used in this study are listed in Table 1. This material was exactly the same as used for previous dynamic tensile tests [4]. The C250 alloy was normalized at 927°C for one hour before water quenching, and then annealed at 816°C for one hour before rapid air cooling. The material was heat treated at 482°C for over 3 hours and then air cooled, making the material with a mean hardness of Rockwell hardness of HRC 48.2 ± 1.3 or a mean yield strength of 1584 ± 43 MPa. The material was then made into cylindrical specimens with a diameter of 6.35 mm and a thickness of 3.18 mm for compression experiments.

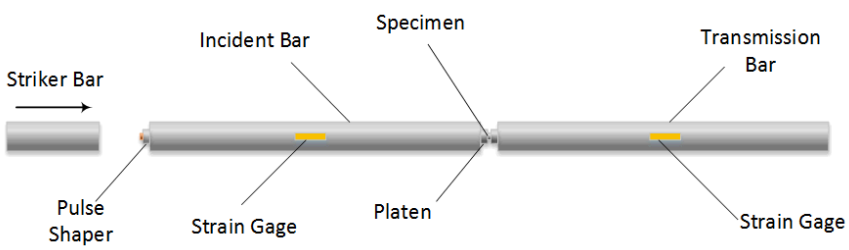

Fig. 1. Schematic of Kolsky compression bar.

3. Dynamic Compressive Experiments

Dynamic compression experiments were conducted with a 25.4-mm-diameter Kolsky compression bar at Sandia National Laboratories. The incident and transmission bars were made of Vascomax®C300 alloy and had a length of 3658 and 2134 mm, respectively. The schematic of the Kolsky compression bar is shown in Fig. 1. Different from conventional Kolsky compression bars, a set of double pulse shapers was placed on the impact end of the incident bar. In this study, the double pulse shaping technique for dynamic compression experiments consists of a small annealed copper stacked on a pre-hardened steel disk. When a striker impacts the double pulse shapers, the piece of soft copper is the first to be plastically deformed, which usually increases the rise time of the incident pulse. When the steel shaper is plastically deformed, the hardening behavior of the steel shaper determines the shape of the

incident pulse. Thus, an incident pulse with specific rise time and shape is generated and propagates in the incident bar. When the incident stress wave propagates to the specimen, part of it is reflected back into the incident bar and the rest transmits into the transmission bar. In this study, the specimens were made of the same material as the pressure bar material but different grades. When a smaller diameter specimen with nearly the same strength as the bar material is subjected to a compression load, the specimen may indent into the pressure bar ends, as mentioned earlier, and generate plastic deformation to the bar ends, which warrants special design of platens placed between the specimen and pressure bars.

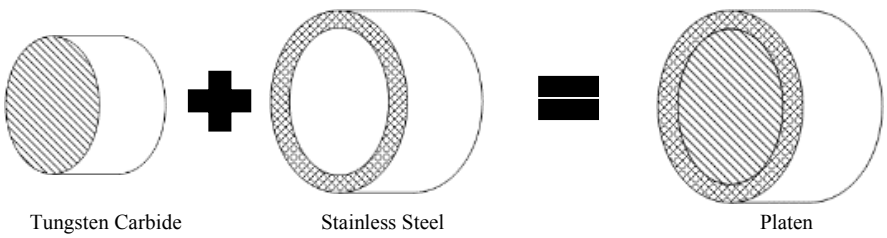

Fig. 2. Design of Platens.

In this study, we selected a tungsten carbide as the platen material. Due to the highly brittle nature of tungsten carbide, a stainless steel sleeve was applied to confine the tungsten carbide, as shown in Fig. 2. However, the tungsten carbide platen with the steel sleeve needs to have nearly identical mechanical impedance as the pressure bars to minimize the disturbance of the stress wave propagation,

$$\left(\rho CA\right)_{platen} = \left(\rho CA\right)_{bar} \tag{1}$$

where ρ is density, C is elastic wave speed, A is cross sectional area. Considering $C = \sqrt{E/\rho}$ where E is Young's modulus, Equation (1) is re-written as

$$\left(\sqrt{\rho E}\,A\right)_{platen} = \left(\sqrt{\rho E}\,A\right)_{bar} \tag{2}$$

For the platen structure shown in Fig. 2, the equivalent density and Young's modulus are calculated as

$$\rho_{platen} = \frac{\rho_{wc} A_{wc} + \rho_s A_s}{A_{platen}} \tag{3}$$

$$E_{platen} = \frac{E_{wc} A_{wc} + E_s A_s}{A_{platen}} \tag{4}$$

where subscripts "*wc*" and "*s*" represent tungsten carbide and stainless steel, respectively. Therefore, the relationship of mechanical impedance match becomes

$$\sqrt{\left(\rho_{wc} A_{wc} + \rho_s A_s\right)\left(E_{wc} A_{wc} + \rho_{wc} A_{wc}\right)} = \left(\sqrt{\rho E}\,A\right)_{bar} \tag{5}$$

The material parameters used for the platen design are listed in Table 2. However, it is noted that the solution for Equation (5) is not unique. In this study, the dimensions of the tungsten carbide disk and the stainless steel sleeve were determined as shown in Table 2. It is noted that the tungsten carbide disk was press fit into the stainless steel sleeve. Table 2 also shows a comparison of mechanical impedance for both platen and pressure bar. As shown in Table 2, the mechanical impedance difference is minimal.

Table 2. Tungsten carbide platen design and mechanical impedance match to the pressure bars

	Material	Density (kg/m^3)	Young's Modulus (GPa)	Diameter (mm)	Thickness (mm)	Mechanical Impedance (kg/s)
Platen	Tungsten Carbide	14450	600	15.00	6.35	
	Stainless Steel	8000	193	18.02 (OD) 15.00 (ID)	6.35	19625 kg/s
Pressure Bars	C300 Maraging Steel	8000	189.9	25.40	N/A	19750 kg/s

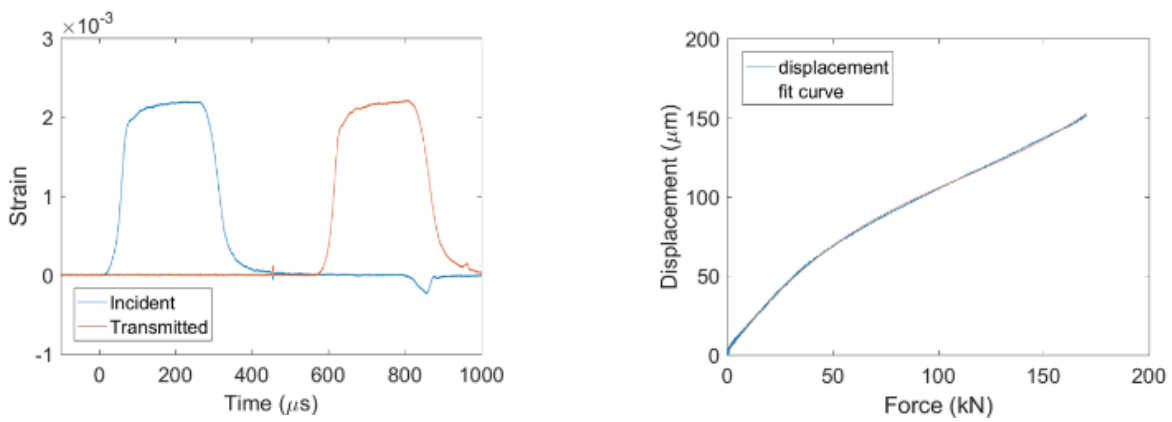

(a) (b)

Fig. 3. Effect of tungsten carbide platens. (a) original oscilloscope signals; (b) force-displacement curve.

In order to check the effectiveness of the tungsten carbide platens, two platens were placed between the pressure bars without any specimen in a Kolsky compression bar experiment. Figure 3(a) shows a typical set of incident, reflected, and transmitted pulses from such a Kolsky compression bar experiment. After the platens are introduced, a small amplitude reflected pulse was observed due to the slight mechanical impedance mismatch between the platens and the pressure bars. This small reflection represents "system compliance" due to the tungsten carbide platens, which may result in erroneous measurement of specimen deformation if not properly corrected. Following the conventional data reduction process, the force and displacement histories of the platens are calculated as

$$F_{platen}(t) = E_{bar} \cdot A_{bar} \cdot \varepsilon_T(t) \tag{6}$$

$$L_{platen}(t) = 2C_{bar}\int_0^t \varepsilon_R(t)dt \tag{7}$$

where ε_R and ε_T are reflected and transmitted bar strains, respectively; E_{bar} and C_{bar} are Young's modulus and elastic wave speed of the bar material, respectively. The force-displacement history of the platens representing "system compliance" is therefore determined and shown in Fig. 3(b). The system compliance needs to be corrected during post processing of Kolsky compression tests of the Vascomax®C250 alloy.

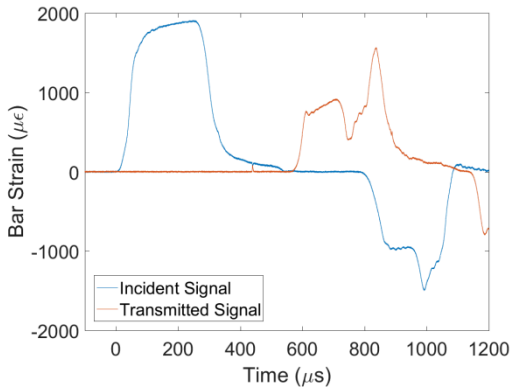

Fig. 4. Oscilloscope signals in a typical Kolsky bar compression bar test.

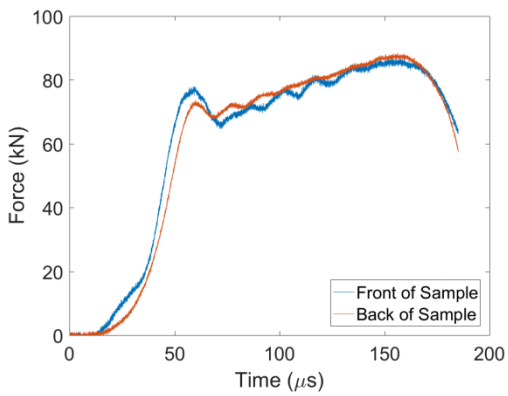

Fig. 5. Dynamic stress equilibrium.

Figure 4 shows a typical set of incident, reflected, and transmitted pulses in Kolsky compression bar experiments on a 6.35-mm-diameter, 3.18-mm-thick Vascomax®C250 alloy specimen. The stresses at both ends of the specimen are calculated as

$$\sigma_{front}(t) = E_{bar}\cdot\left(\varepsilon_I(t)+\varepsilon_R(t)\right)\cdot\frac{A_{bar}}{A_{specimen}} \tag{8a}$$

$$\sigma_{back}(t) = E_{bar}\cdot\varepsilon_T(t)\cdot\frac{A_{bar}}{A_{specimen}} \tag{8b}$$

where ε_I is the incident strain in the incident bar; A_{bar} and $A_{specimen}$ represent the cross-sectional areas of the pressure bars and the specimen, respectively. The stress equilibrium process is shown in Fig. 5. Through proper pulse shaping technique, the specimen stress approaches to equilibrium at ~40 microseconds. The displacements at both ends of the specimen are calculated as

$$L_{front}(t) = C_{bar}\int_0^t \left(\varepsilon_I(t)-\varepsilon_R(t)\right)dt \tag{9}$$

$$L_{back}(t) = C_{bar}\int_0^t \varepsilon_T(t)dt \tag{10}$$

Therefore, the relative displacement is

$$L_{measure}(t) = C_{bar}\int_0^t (\varepsilon_I(t) - \varepsilon_R(t) - \varepsilon_T(t))dt \tag{11}$$

It is noted that the relative displacement calculated with Eq. (11) includes the system compliance (Eq. (7)) which needs to be removed. Furthermore, even though a pair of tungsten carbide platens are applied to avoid plastic indentation, elastic indentation of the specimen into the tungsten carbide platens may still occur. The displacement associated with elastic indentation was given by Safa and Gary [13]

$$L_{indentation}(t) = 2\cdot F(t)\cdot\frac{16}{3\pi^2}\cdot\frac{1-\upsilon^2}{d\cdot E}\cdot H_p\left(\frac{d}{D}\right) \tag{12}$$

where, in this study, υ is Poisson's ratio of the tungsten carbide platens; d and D are diameters of the specimen and tungsten carbide platens, respectively. The function of H_p was also provided by Safa and Gary [13]. The displacement over the specimen is thus calculated and also used for specimen strain calculation,

$$\varepsilon(t) = \frac{L_{measure} - L_{platen} - L_{indentation}}{L_{specimen}} \tag{13}$$

where $L_{specimen}$ is the specimen length.

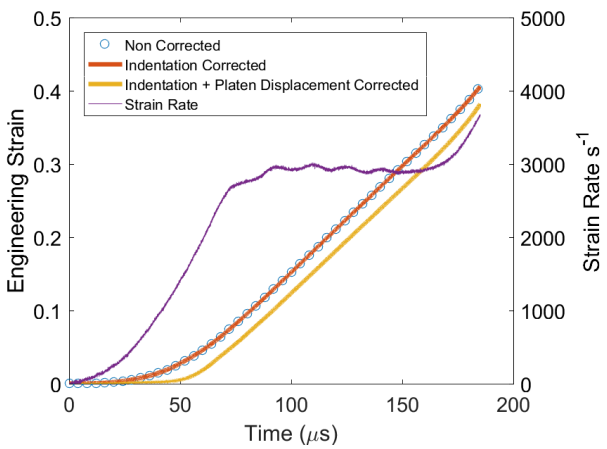

Fig. 6. Engineering strain and strain rate histories.

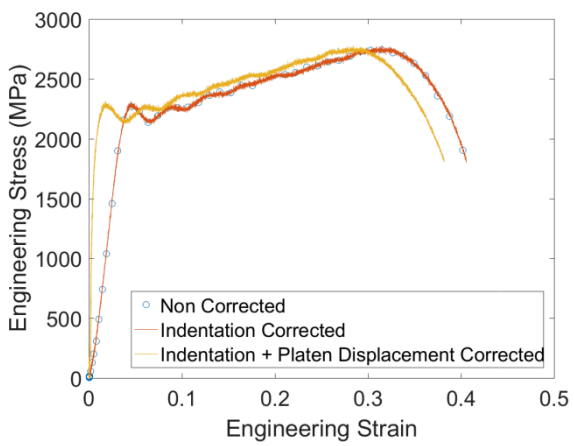

Fig. 7. Engineering stress-strain curves with and without corrections.

Figure 6 shows a comparison of specimen strain histories with and without corrections. It is seen that the strain histories without correction and with indentation correction are overlapped, meaning that the indentation effect is negligible due to very high stiffness of the tungsten carbide platens. However, the addition of the tungsten carbide platens significantly overestimates the specimen strain particularly at small strains, which must be corrected. Also shown in Fig. 6 is he strain rate of the specimen, calculated by differentiating Eq. (13). As shown in Fig. 6, the specimen was deformed at a nearly constant strain rate of 3000 s^{-1} until it was fractured at ~ 170 μs. When the specimen was fractured, the sudden loss of load-bearing capacity caused the strain-rate jump (Fig. 6).

From the engineering stress and strain histories calculated with Equations (8) and (13), respectively, the engineering stress-strain curve was obtained by eliminating the time. Figure 7 shows a comparison of engineering stress-strain curves of the specimen material with and without corrections. The correction of platen displacement significantly changes the elastic portion, particularly the Young's modulus, in the engineering stress-strain curve. Again, the indentation has a negligible effect on the stress-strain response in this study.

Assuming the specimen material is incompressible and taking compressive stress and strain as positive, the true compressive stress-strain curve is calculated from engineering measurements with the following equations,

$$\sigma_{True}(t) = \sigma_{Eng} \cdot \left(1 - \varepsilon_{Eng}\right) \tag{14a}$$

$$\varepsilon_{True}(t) = -\ln\left(1 - \varepsilon_{Eng}\right) \tag{14b}$$

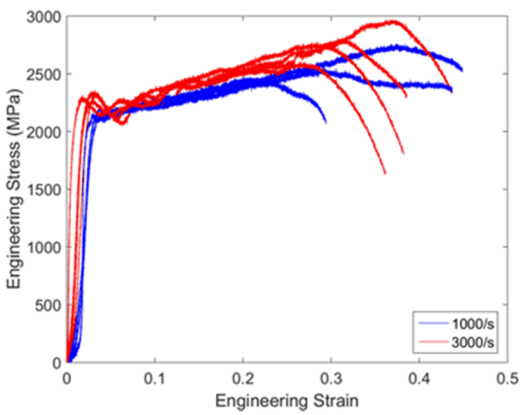

Fig. 8. Engineering stress-strain curves in dynamic compression.

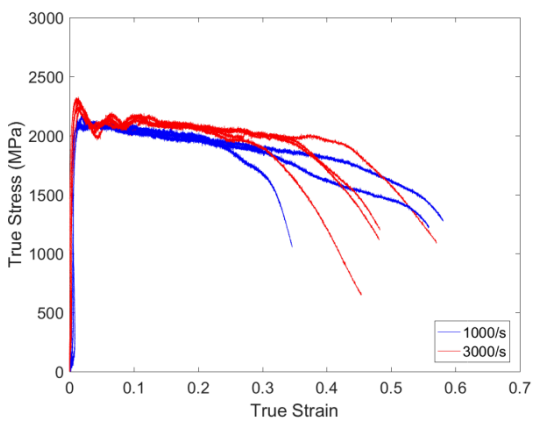

Fig. 9. True stress-strain curves in dynamic compression.

4. Experimental Results and Discussion

Following the same procedure, dynamic engineering compressive stress-strain curves of Vascomax®C250 alloy were obtained at two different strain rates: ~1000 and 3000 s^{-1}, shown in Fig. 8. At each strain rate, 3-4 experiments were repeated. The dynamic engineering stress-strain curves exhibit a typical elastic and work hardening behavior with a reasonable repeatability. When the strain rate increases from 1000 to 3000 s^{-1}, the flow stress increased by ~10%. The dynamic yield strength was also approximately 18% higher than quasi-static yield strength. All these

represent strain rate effect of the Vascomax®C250 alloy. Under dynamic compression, the specimens were fractured at ~0.30 in engineering strain. The fracture strain shows little strain-rate dependency. Figure 9 shows the true stress-strain curves in dynamic compression, which were calculated with Equations (14a) and (14b). The true compressive stress-strain curves possess an elasticity followed by a slight softening behavior.

In order to check the symmetry of dynamic compression and tension response, the averaged true stress-strain curves in compression were calculated and compared with the previously-obtained tensile true stress-strain curves in tension [4] for the same material and at the same strain rates. The comparison result is shown in Fig. 10. Since necking occurs at small strains (~10%) for the Vascomax®C250 alloy under dynamic tension [4], the true tensile stress-strain curve is only reliable for the first 10% strain. However, the true stress and strain at fracture were calculated with Bridgman correction based on the geometry and dimensions of the fractured specimen after dynamic tensile test. The true tensile stress-strain curves between necking and fracture were not able to be determined and therefore were replaced with dash lines. As shown in Fig. 10, at the same dynamic strain rate, the Vascomax®C250 alloy exhibits reasonable symmetry in compression and tension in terms of yield and early plastic flow response. However, the material possessed smaller fracture strains in compression than in tension. This is probably due to different instability and fracture mechanisms of the material when subjected to different loading modes (compression or tension).

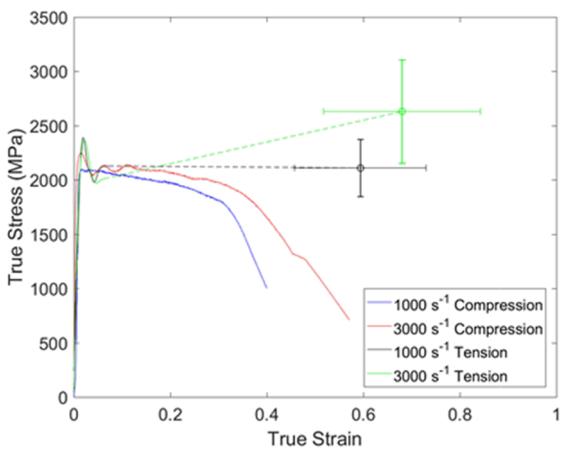

Fig. 10. Comparison of true compressive and tensile stress-strain curves.

5. Conclusions

A Kolsky compression bar was employed to dynamically characterize the compressive stress-strain response of Vascomax®C250 alloy in compression at two high strain rates: 1000 and 3000 s^{-1}. In order to prevent the pressure bar ends from being indented by the high-strength specimen, a tungsten carbide disk was press fit into a stainless steel sleeve to construct a high-stiffness, high strength platen which was placed between the specimen and pressure bar. The tungsten carbide platen was carefully designed to match the mechanical impedance to the pressure bars. However, there still existed a small disturbance of stress wave propagation, which represented "system compliance" caused by the platens. The displacement of platens during dynamic compressive loading were calibrated and the resultant "system compliance" was removed from the original specimen strain measurements. Elastic indentation of the high-strength specimen into the tungsten carbide platens was also evaluated. The results showed that such elastic indentation was negligible due to superior stiffness of the tungsten carbide platens. A double-pulse-shaping technique was employed to facilitate stress equilibrium and constant strain rate in the specimen. The resultant compressive stress-strain curves of the Vascomax®C250 alloy were observed to be strain-rate dependent. The

dynamic yield strength of the Vascomax®C250 alloy was approximately 18% higher than quasi-static yield strength. Even within dynamic strain-rate range, the flow strength of the Vascomax®C250 alloy at 3000 s^{-1} was approximately 10% higher than that at 1000 s^{-1}. The dynamic compressive stress-strain response was also compared to the dynamic tensile stress-strain response at the same strain rates. The results showed that the Vascomax®C250 alloy possessed reasonable symmetry in dynamic compression and tension, except for the strains at fracture. The dynamic fracture strains in compression were observed smaller than those in dynamic tension, which was probably due to different fracture mechanisms under different loading modes.

Acknowledgements

Sandia National Laboratories is a multi-program laboratory managed and operated by Sandia Corporation, a wholly owned subsidiary of Lockheed Martin Corporation, for the U.S. Department of Energy's National Nuclear Security Administration under contract DE-AC04-94AL85000.

References

[1] www.atimetals.com
[2] H. Kolsky, An investigation of the mechanical properties of materials at very high rates of loading, Proc. Phys. Soc. London B62 (1949) 676-700.
[3] J. Harding, E.O. Wood, J.D. Campbell, Tensile testing of materials at impact rates of strain, J. Mech. Eng. Sci. 2 (1960) 88-96.
[4] B. Song, P.E. Wakeland, M. Furnish, Dynamic tensile characterization of Vascomax® maraging C250 and C300 alloys, J. Dynamic Behavior Mater. 1 (2015) 153-161.
[5] B. Song, B.R. Antoun, Pseudo stress response in Kolsky tension bar experiments, Exp. Mech. 52 (2012) 525-528.
[6] B. Song, B.R. Antoun, H. Jin, Dynamic tensile characterization of a 4330-V steel with Kolsky bar techniques, Exp. Mech. 53 (2013) 1519-1529.
[7] Y. Qiu, C.M. Loeffler, X. Nie, B. Song, Improved experimental and diagnostic techniques for dynamic tensile stress-strain measurement with a Kolsky tension bar, (to be submitted).
[8] X. Nie, B. Song, C.M. Loeffler, A novel splitting-beam laser extensometer technique for Kolsky tension bar experiment, J. Dynamic Behavior Mater. 1 (2015) 70-74.
[9] W. Chen, B. Song, Split Hopkinson (Kolsky) bar: design, testing and applications, Springer, New York, 2011.
[10] D.J. Frew, M.J. Forrestal, W. Chen, Pulse shaping techniques for testing brittle materials with a split Hopkinson pressure bar, Exp. Mech. 42 (2002) 93-106.
[11] D.J. Frew, M.J. Forrestal, W. Chen, Pulse shaping techniques for testing elastic-plastic materials with a split Hopkinson pressure bar, Exp. Mech. 45 (2005) 186t-195.
[12] G. Ravichandran, G. Subhash, Critical appraisal of limiting strain rates for compression testing of ceramics in a split Hopkinson pressure bar, J. Amer. Ceram. Soc. 77 (1994) 263-267.
[13] K. Safa, G. Gary, Displcement correction for punching at a dynamically loaded bar end, Int. J. Impact Eng. 37 (2010) 371-384.
[14] B. Song, E. Nishida, E. Corona, Data-reduction uncertainties in Kolsky bar experimetns on metals, 2015 SEM Annual Conference & Exposition on Experimental & Applied Mechanics, June 8-11, 2015, Costa Mesa, California, USA.
[15] W. Chen, G. Ravichandran, Dynamic compressive behavior of a glass ceramic under lateral confinement. J. Mech. Phys. Solids 45 (1997) 1303-1328.